Electric Power Systems Research 207 (2022) 107848

Contents lists available at ScienceDirect

Electric Power Systems Research

journal homepage: www.elsevier.com/locate/epsr

Dynamic interactions in large scale photovoltaic power plants with frequency and voltage support

Ruben Salazar-Chiralt [a], Marc Cheah-Mane [a,*], Elia Mateu-Barriendos [a], Eduard Bullich-Massague [a], Eduardo Prieto-Araujo [a], Hasan Mehrjerdi [b], Oriol Gomis-Bellmunt [a]

[a] CITCEA, Universitat Politecnica de Catalunya, 647 Diagonal Avenue, Barcelona 08028, Spain
[b] Department of Electrical Engineering, College of Engineering, Qatar University, University Street, Doha 2713, Qatar

ARTICLE INFO

Keywords:
Large scale photovoltaic power plant
Power plant controller
Small-signal analysis
Stability
Dynamic interactions

ABSTRACT

The increasing penetration of Large-Scale Photovoltaic Power Plants in the power system is raising the concern of potential stability issues due to dynamic interactions of power electronics components. In particular, Power Plant Controllers are starting to provide a fast dynamic response for specific services, such as fast frequency response, which could trigger unexpected unstable interactions with the PV inverters or other grid components. Also, an eventual reduction of synchronous generation in the grid could lead to a power system with high penetration of power electronics, which presents unexplored stability problems. This paper presents an interaction and stability study of a Photovoltaic Power Plant connected to the grid. This study is based on a small-signal analysis employing eigenvalues and participation factors to identify potential unstable modes. A linear model of the Photovoltaic Power Plant is implemented to apply a small-signal analysis. This linear model is validated with the equivalent non-linear model based on time-domain simulations in Matlab Simulink.

1. Introduction

Solar photovoltaic (PV) is one of the renewable energies with the highest potential due to the massive solar resource available and the maturity that PV generation technologies have achieved. The considerable price reduction that PV technologies have experienced during the past years [1], have led to a fast and massive deployment of PV power plants (PVPP) worldwide. In particular, Large-scale Photovoltaic Power Plants (LSPVPP) represent around 66% of the of the PV installations by capacity LS-PVPP can have an important impact on the overall power system, and they have to fulfil the grid codes to ensure a smooth grid integration and system stability. Nowadays, due to the fast growth that PV has experienced, the impact that LS-PVPP can have on the grid stability is a concern for different system operators worldwide. Modern grid codes [2,3] include specific requirements considering the special nature of renewable power plants, especially solar and wind. The trend is to have more demanding grid codes, including additional services and requiring faster dynamics for the services provided. This has led to the implementation of new grid services, such as Fast Frequency or Support (FFR) [4–6], Power Oscillation Damping (POD) [5] and power fluctuation smoothing control [7] or the upgrade of existing ones such as the Fault-ride-through (FRT) [8].

In addition, the increasing penetration of renewable sources in the power system is resulting in the replacement of synchronous generation (SG) in favour of power electronics units, especially voltage source converters (VSC). This scenario is especially critical for islanded systems as presented in Nanou et al. [6], Rosini et al. [9]. Then, power systems with high penetration of converters might require alternative control design and structures as the system stability can be compromised. For example, the damped-SOGI-based Control is presented in Singh et al. [10] and the Model Predictive Control is applied for the frequency and voltage support in Rosini et al. [9], Armendáriz et al. [11].

Also, the stability issues in power systems with high penetration of power electronics are mostly related with control interaction between different parts of the system [5,6,12,13]. Stability can be analysed based on transient analysis as presented in Crăciun et al. [4], Varma and Akbari [5], Singh et al. [13] or small-signal analysis as presented in Nanou et al. [6], Liu et al. [12]. Small-signal analysis is not valid for large disturbances, but provides an analytical stability evaluation with different methods, such as the eigenvalues or the participation factors analysis. These methods are useful to identify the source of instability and design a solution.

* Corresponding author.
E-mail address: marc.cheah@upc.edu (M. Cheah-Mane).

https://doi.org/10.1016/j.epsr.2022.107848
Received 21 May 2021; Received in revised form 30 January 2022; Accepted 3 February 2022
Available online 8 February 2022

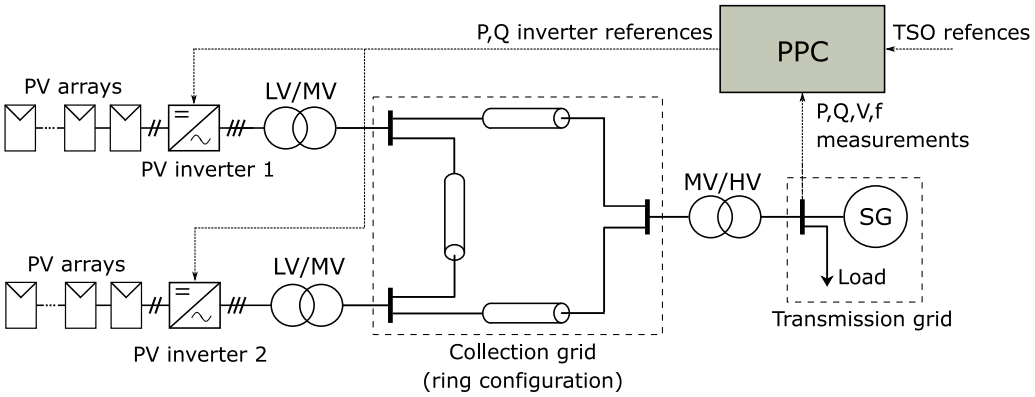

Fig. 1. General scheme of LS-PVPP scheme with two PV inverters.

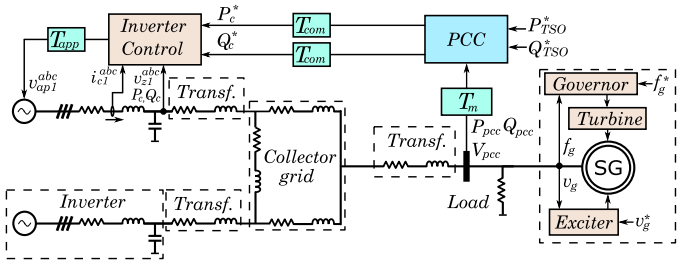

Fig. 2. Electric circuit and modelled blocks of LS-PVPP scheme with two PV inverters.

The PVPP can be controlled with a centralized [4,14] or decentralized structure [9,14]. A centralized Power Plant Controller (PPC) is typically considered for LS-LVPP. The frequency control is implemented as a centralized option for PVPPs connected to the transmission grid [4,5], while the decentralized option is for PVPPs connected to microgrids [9,13]. The voltage control is typically analyzed as a decentralized option for PVPPs connected to microgrids [9,13] or the distribution grid [9,11,15]. However, voltage control is also implemented with a centralized structure for LS-PVPPs due to the grid code requirements at the point of connection.

The stability analysis can be focused on the PVPP grid or the PVPP connection to a power system. If the analysis is focused on the main dynamic interactions within the LS-PVPP, a Thevenin equivalent grid is sufficient [6]. However, if interactions with the grid are analyzed a more detailed representation must be considered [12]. The PVPP is usually represented as a single-PV generator, without providing details of the PVPP grid or the PPC [5,6,8,10,12].

This paper is oriented to understand the dynamic interactions in a LS-PVPP, considering the dynamics of the grid, the PV inverters and the PCC. The provision of frequency and voltage support to the main grid is considered. The main contributions of the paper are:

- Implementation of small-signal model for a reduced PVPP considering the PV inverters, collection grid, transformers and PPC. The existing small-signal models presented in the literature consider a single-PV generator representation [4,10].
- Identification of dynamic interactions within a PVPP and with the grid, based on eigenvalue and participation factor analysis, which provides a better understanding of the interaction phenomenon. In particular, interactions due to the frequency and voltage control implemented in the PPC are analysed in detail. In the literature, interactions are usually analysed mainly based on transient analysis [5,9,13].
- Evaluation of dynamic interactions for power systems with reduced synchronous generation, i.e. high integration of PV generation with power electronics components. In the literature, PVPP integration in standard IEEE models with SG components is considered [4,5,8,12,14], but only in Liu et al. [12] an eventual replacement of the SGs by PVPPs is analysed.

The grid is represented as an aggregated synchronous generator and a load, which is sufficient to analyse the essential interactions due to voltage and frequency controls of the PPC. A similar approach was considered in Collados-Rodriguez et al. [16] to analyse the interactions between a VSC and a SG.

The rest of the paper is organized as follows. The PVPP model is presented in Section 2, to better understand the LS-PVPP and to comprehend its role in the power system. Such model is linearised and expressed in state-space form to perform a dynamic analysis based on eigenvalues, to study the stability of the system, and participation factors, to figure out the interactions existing in the system. Section 3 introduces the interaction and stability analysis, where several scenarios are studied. First, an initial case study is presented, where the PPC is based on active and reactive control loops. Then, the introduction of the grid frequency and voltage support is considered. Finally, an additional scenario is studied considering a reduction of synchronous generation, which is equivalent to consider a high penetration of PV generation.

2. Large-scale PV power plant model

2.1. System description

A LS-PVPP is formed by a number of PV inverters connected to a medium voltage (MV) collection grid that transfers the generated power to the high voltage (HV) transmission grid. The PV inverters generate power in low voltage (LV) and are connected to MV through a LV/MV set-up transformer, while the collection grid is connected to HV through an MV/HV set-up transformer. The collection grid can have different configurations, but ring topology is selected, since represents a common option for LS-PVPP. A PPC is included to ensure that active and reactive powers are regulated at the point of connection following the grid code power references and other requirements.

The general scheme of the LS-PVPP model is shown in Fig. 1, while the electrical circuit and the modelled blocks are shown in Fig. 2. As the main purpose of this study is to analyse the interactions and stability of the PPC, an aggregated model of the LS-PVPP is considered with a reduced number of PV inverters. In particular, the power plant includes two aggregated PV inverters. This representation is supposed to be sufficient to represent the collection grid and the PV inverter control dynamics.

2.2. PV power plant

The PV power plant model includes the PPC, the PV inverters, the

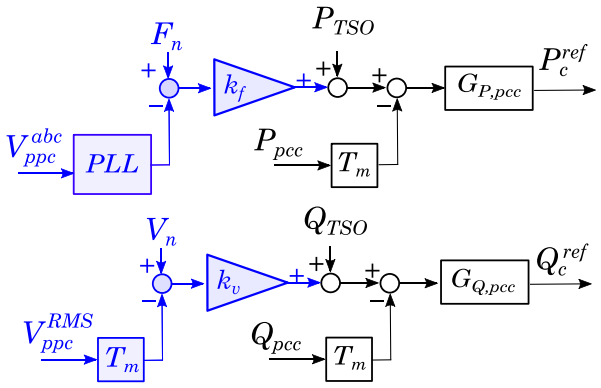

Fig. 3. Structure of PPC with inner active and reactive power control and outer frequency and voltage controls.

collection grid and the transformers.

2.2.1. PPC

The PPC is based on a central control structure, which ensures that grid code requirements from the TSO are accomplished at the point of connection of the PV plant. The control structure is based on a cascaded control that includes active and reactive power controls as inner loops and voltage and frequency controls as outer loops (see Fig. 3). The PPC power controls are implemented as Proportional-Integral (PI) controllers and provide the power references for the PV inverters. In particular, the same power references are sent to all the inverters. The frequency and voltage controls are implemented as proportional controllers, which is usually defined in the grid codes. The frequency is measured with a PLL, while the voltage is measured as an RMS value. The control gains of the frequency and voltage support are defined with the following expressions:

$$k_f = \frac{S_n}{f_n R_f}; \quad k_v = \frac{S_n}{f_n R_v} \tag{1}$$

where S_n is the nominal power of the plant and R_f and R_v are the droop percentages.

The PPC response also depends on the communications with the PV inverters, the measurements and the sampling process. Therefore, the effect of communications, measurement and PPC sampling delays is modeled using a first order Padé approximation, which is a sufficient representation if high frequencies are not analyzed. Then, all delays are expressed as follows:

$$T_i = \frac{-\tau_i/2 \cdot s + 1}{\tau_i/2 \cdot s + 1} \tag{2}$$

where τ_i is the delay time for each i-component.

2.2.2. PV inverter

The PV inverters are represented with average models of 2-level Voltage Source Converters (VSC). The VSCs are responsible for controlling the active and reactive power references sent by the PPC. In particular, the VSCs regulate the DC voltage, such that the PV panels can provide the required active power. However, the dynamic response of the PV panels can be considered to be decoupled from the AC grid. Therefore, the DC side of the VSCs is not modelled and the DC voltage control is replaced by an active power control.

The VSC control structure is shown in Fig. 4. The control is implemented in a qd0 frame and is based on a typical cascaded structure, with an inner current loop and an outer power control. Both the current and the power controls are implemented as PI controllers. A Phase-locked Loop (PLL) is required to track the grid angle and ensure that currents and voltages are represented in a qd0 frame. In addition, an application delay is included to represent the effect of sampling and modulation at the voltage applied by the VSC. This delay is modelled as a first order Pade approximation in (2).

2.2.3. Collection grid and transformers

The collection grid and transformers are represented as impedances interconnected at the same voltage level as shown in Fig. 2. In particular, the whole LS-PVPP is represented at the MV level. The MV cables of the collection grid are modeled as RL circuits, which is a sufficient representation since they have a short length, usually less than 1 km. The transformers are also represented as RL circuits, assuming that the core model is neglected.

2.3. Main grid

The main transmission grid is modelled as a SG with a load, which enables the analysis of frequency and voltage support implemented in the PPC.

The SG model considers the electrical circuits of the generator, the turbine and the exciter and governor systems, as shown in Fig. 2. The electrical circuits are represented in qd0 frame, assuming a round rotor and including the following elements: stator windings, field windings and three damper windings. Also, the turbine dynamics of a thermal generation plant are represented, which consider the generator's inertia, the high and low pressures turbines and a reheater. The exciter system is used to control the AC grid voltage. This control is based on a proportional controller, where the output is an excitation voltage applied in the field windings. The exciter system implemented in the model is the IEEE type AC4A [17]. The governor system is used to provide frequency support. This control is also implemented as a proportional controller, where the output is the active power variation required to regulate the frequency. More details about this SG model can be found in Collados-Rodriguez et al. [16].

The electric load is represented as a resistance that consumes a

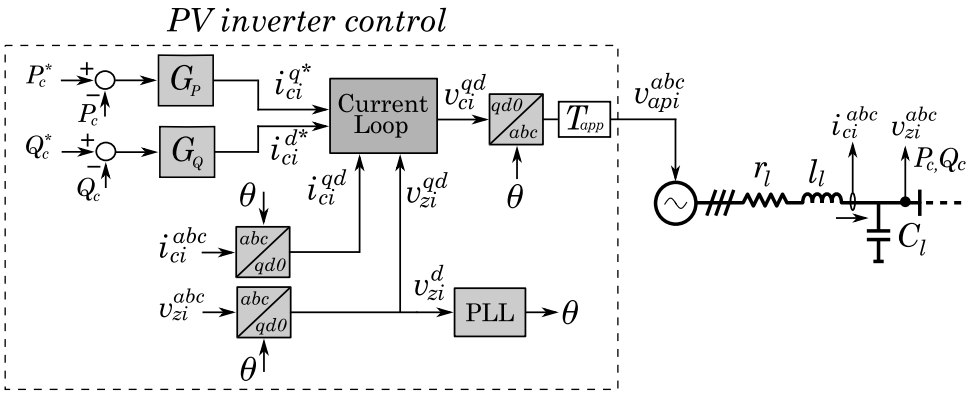

Fig. 4. PV inverter control structure.

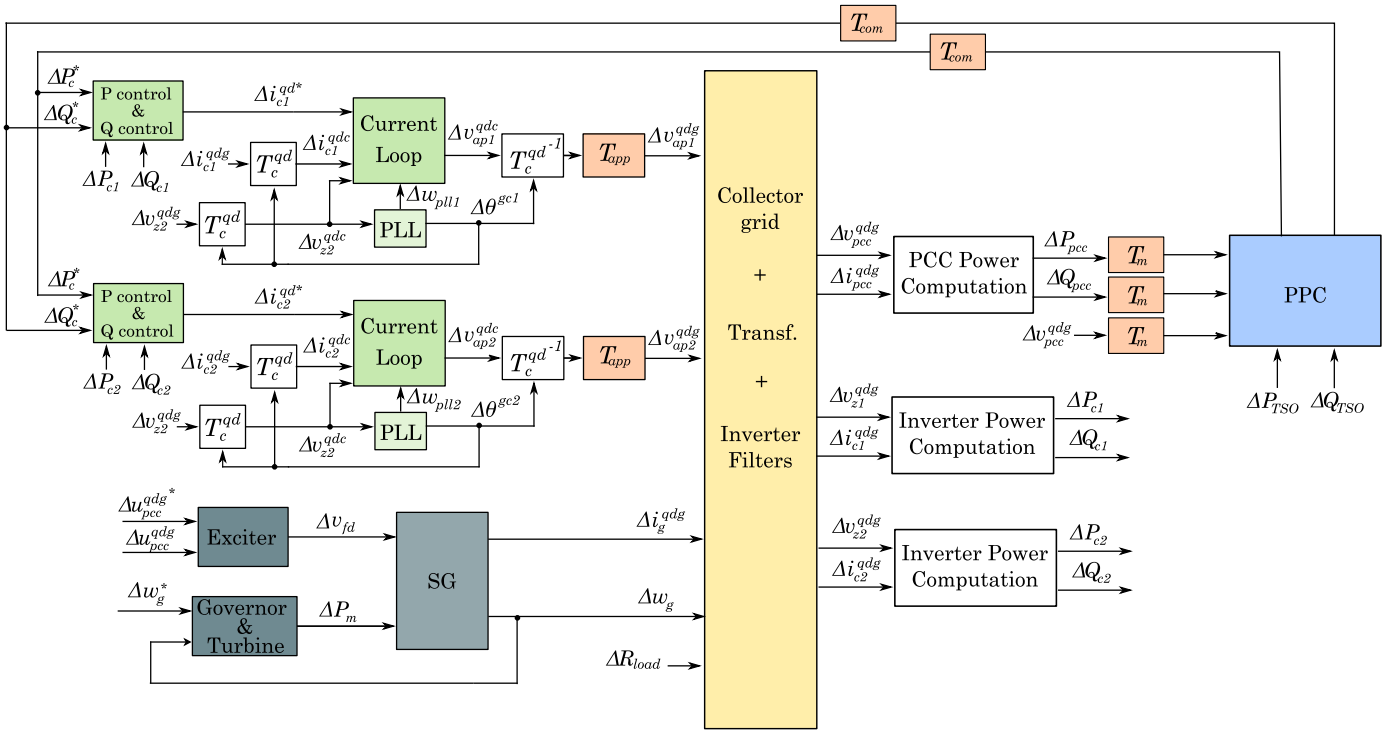

Fig. 5. Complete block diagram for state-space representation of the LS-PVPP with two inverters.

specific active power at nominal voltage. The load is connected at the same bus as the synchronous generator and the LS-PVPP as seen in Fig. 2.

2.4. Linear model

2.4.1. Model definition

A linear model of the LS-PVPP is implemented to analyse interactions and stability due to small-signal variations. The linear model is implemented in a qd0 frame, enabling a simple formulation of the electrical equations. The model is divided in different qd0 frames depending on the angle where the Park transformation is applied. Considering the model with two inverters in Fig. 2, three reference frames are defined:

- SG-Reference Frame (SG-RF): this frame is aligned to the SG angle and includes the following components: the SG, the load, the collection grid, the transformers and the VSC filters.
- VSC1 and VSC2-Reference Frames (VSC1 and VSC2-RF): these frames are aligned to the PLL angle of each VSC and include the inverter controls.

The subsystems expressed in different reference frames are interconnected employing rotation transformations to current and voltage variables. In particular, these transformations are always between VSC and SG frames. Then, the rotation transformation is linearised as follows:

$$\left[\Delta x^{qci}, \Delta x^{dci}\right]^T = \mathbf{T_c}\left[\Delta x^{qg}, \Delta x^{dg}, \Delta\theta^{gci}\right]^T \tag{3}$$

$$\mathbf{T_{gc}} = \begin{bmatrix} \cos\theta_0^{gci} & -\sin\theta_0^{gci} & -x_0^{qg}\sin\theta_0^{gci} - x_0^{dg}\cos\theta_0^{gci} \\ \sin\theta_0^{gci} & \cos\theta_0^{gci} & x_0^{qg}\cos\theta_0^{gci} - x_0^{dg}\sin\theta_0^{gci} \end{bmatrix} \tag{4}$$

where x^{qci} and x^{dci} are the variables expressed in each VSCi-RF, x^{qg} and x^{dg} are the variables expressed in the SG-RF and θ^{gci} is the angle difference between SG-RF and each VSCi-RF. The subindex 0 is referred to initial values for the variables.

Fig. 5 shows a representation of the complete linear model for the LS-PVPP with two inverters, which is formed by subsystems that represent different linear state-space blocks interconnected among them. As a result, the complete model can be represented in the following state-space structure:

$$\dot{\mathbf{x}}_\mathbf{T} = \mathbf{A_T}\cdot\mathbf{x} + \mathbf{B_T}\cdot\mathbf{u_T}; \quad \mathbf{y_T} = \mathbf{C_T}\cdot\mathbf{x} + \mathbf{D_T}\cdot\mathbf{u_T}; \tag{5}$$

where $\mathbf{x_T}$ is the vector of all state variables, $\mathbf{u_T}$ is the vector of all inputs and $\mathbf{y_T}$ is the vector of all outputs.

The total number of state variables for a PV plant with two inverters is equal to 48. These states can be divided in different groups that will be used in the interaction analysis to identify the elements that participate on each mode. In particular the following groups are defined:

- Collection grid (14 states): currents ($i_{c1}^q, i_{c1}^d, i_{c2}^q, i_{c2}^d, i_{12}^q, i_{12}^d, i_g^q, i_g^d$) and voltages ($v_{z1}^q, v_{z1}^d, v_{z2}^q, v_{z2}^d, v_g^q, v_g^d$).
- VSC control (12 states): current loop ($S_{eiq1}, S_{eid1}, S_{eiq2}, S_{eid2}$), power loop ($S_{eP1}, S_{eP2}, S_{eQ1}, S_{eQ2}$) and PLL ($\omega_{pll1}, \omega_{pll2}, \theta^{gc1}, \theta^{gc2}$)
- PPC (3 states): power control (S_{ePPC}, S_{eQPPC}) and PLL (ω_{pllPPC})
- Delays (9 states): VSC application ($v_{ap1}^q, v_{ap1}^d, v_{ap2}^q, v_{ap2}^d$), measurements ($P_{ppc}^{del}, Q_{ppc}^{del}, V_{ppc}^{del}$) and communications + PPC sampling (P_c^{*del}, Q_c^{*del})
- SG (10 states): governor (ST_m), exciter (S_{ex}^1, S_{ex}^2) and electrical circuits ($i_s^q, i_s^d, i_f^d, i_k^d, i_{k1}^q, i_{k2}^q, \omega_g$)

In addition, the input vector $\mathbf{u_T}$ is defined with the following groups:

- Resistive load (R_{load})
- PPC references from TSO ($P_{TSO}, Q_{TSO}, V_{TSO}, \omega_{TSO}$)
- Reference frequency of governor (ω_g^*)

2.4.2. Model validation

The linear model is validated against the non-linear model applying an input variation of 1%, which is a typical value used to excite the modes in a small-signal range. In particular, a load step R_{load} is applied at

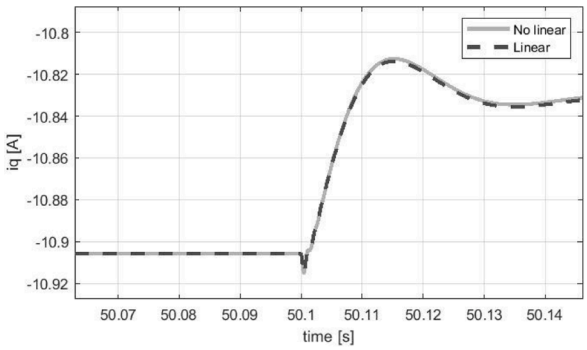

(a) i_{c1}^{q}

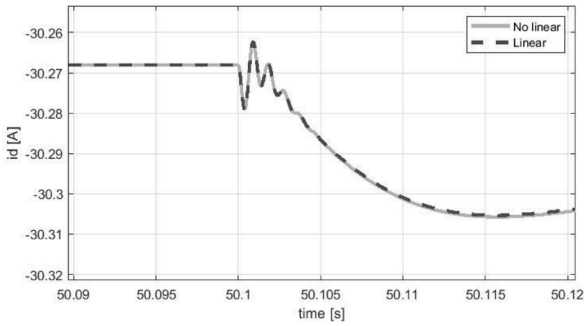

(b) i_{c1}^{d}

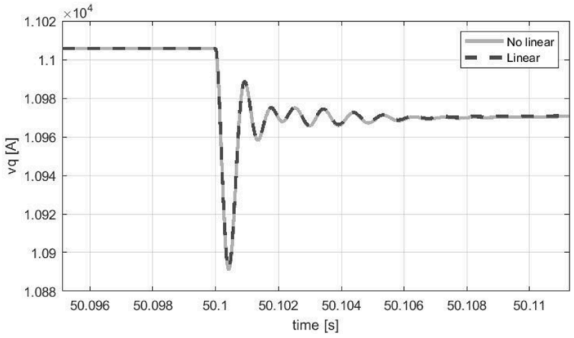

(c) v_{z1}^{q}

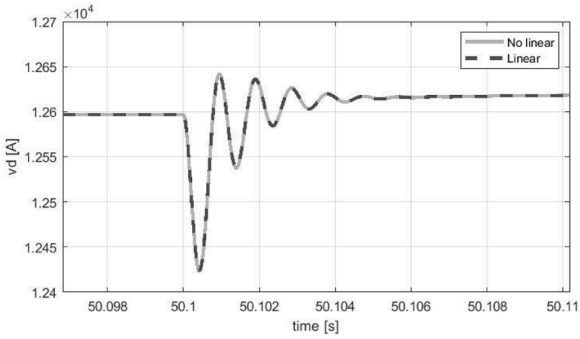

(d) v_{z1}^{d}

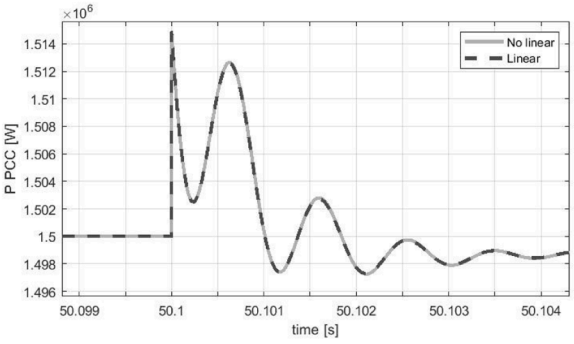

(e) P_{ppc}

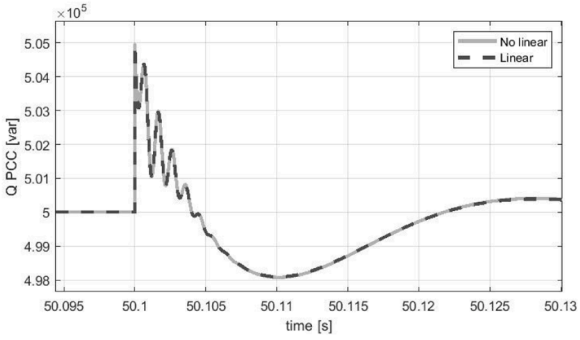

(f) Q_{ppc}

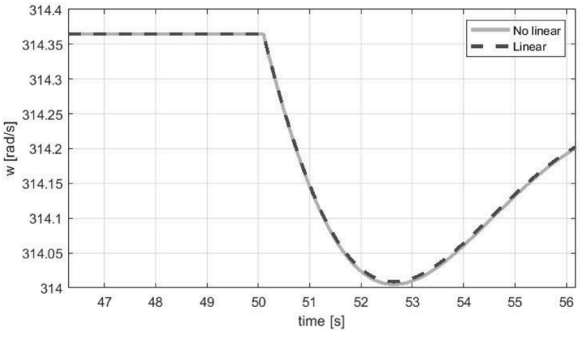

(g) ω_g

Fig. 6. Time-domain simulations to validate the linear model against the non-linear model for a R_{load} variation.

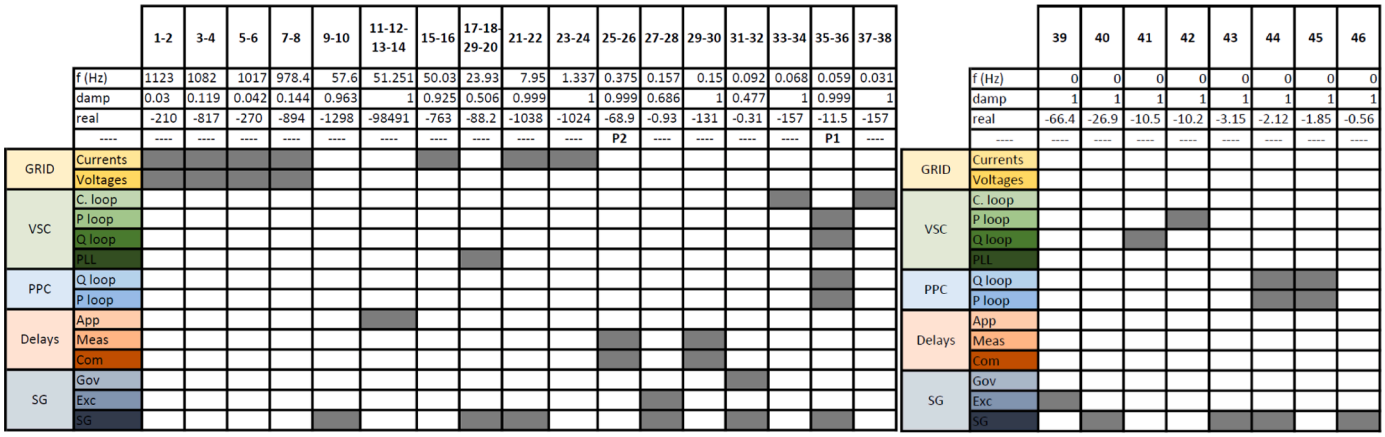

		1-2	3-4	5-6	7-8	9-10	11-12-13-14	15-16	17-18-29-20	21-22	23-24	25-26	27-28	29-30	31-32	33-34	35-36	37-38
	f (Hz)	1123	1082	1017	978.4	57.6	51.251	50.03	23.93	7.95	1.337	0.375	0.157	0.15	0.092	0.068	0.059	0.031
	damp	0.03	0.119	0.042	0.144	0.963	1	0.925	0.506	0.999	1	0.999	0.686	1	0.477	1	0.999	1
	real	-210	-817	-270	-894	-1298	-98491	-763	-88.2	-1038	-1024	-68.9	-0.93	-131	-0.31	-157	-11.5	-157
	----	----	----	----	----	----	----	----	----	----	----	P2	----	----	----	----	P1	----
GRID	Currents																	
	Voltages																	
VSC	C. loop																	
	P loop																	
	Q loop																	
	PLL																	
PPC	Q loop																	
	P loop																	
Delays	App																	
	Meas																	
	Com																	
SG	Gov																	
	Exc																	
	SG																	

(a) Oscillatory modes

		39	40	41	42	43	44	45	46
	f (Hz)	0	0	0	0	0	0	0	0
	damp	1	1	1	1	1	1	1	1
	real	-66.4	-26.9	-10.5	-10.2	-3.15	-2.12	-1.85	-0.56
	----	----	----	----	----	----	----	----	----
GRID	Currents								
	Voltages								
VSC	C. loop								
	P loop								
	Q loop								
	PLL								
PPC	Q loop								
	P loop								
Delays	App								
	Meas								
	Com								
SG	Gov								
	Exc								
	SG								

(b) Non-oscillatory modes

Fig. 7. List of LS-PVPP modes and significant PF contribution for the initial case study when only active and reactive power control are analyzed.

50.1 s, which results in the dynamic responses shown in Fig. 6 for different variables of the VSC1 (currents, voltages and powers), the SG (currents and grid frequency) and the PPC (powers). Since VSC1 and VSC2 have the same parameters, the results are identical and only VSC1 results are shown. It is clear that the linear and non-linear models have an adequate matching and the linear model is able to capture the dynamic oscillations from the non-linear model. Therefore, the linear model is valid for the small-signal analysis presented in the following Section.

3. Interaction and stability analysis

3.1. General methodology and case studies

In this section, the stability and interaction analysis of the system is presented, which is based on a small-signal analysis employing the linear model presented in Section 2.4. Small-signal analysis can be used for small disturbances in the system derived from the normal evolution and operation of the system, such as load or generation variation and modifications in the grid configuration. Non-linear models can be also use to identify small disturbance interactions from time-domain simulations, but the computation time is higher than in linear-models, especially for complex dynamic models. When transient events, such as faults or large generator and load disconnections, are considered linear models are not valid and only non-linear models can capture the dynamic interactions employing standard approaches as parametric time-domain simulations.

As part of the small-signal analysis, the eigenvalues and participation factors (PFs) are mathematical tools that can be derived from the state-space linear models and provide detailed information about the dynamic interactions. In this section, the dynamic analysis of the system is presented, which is based on an interaction and stability analysis with eigenvalues and participation factors (PFs).

The eigenvalues are extracted from the $\mathbf{A_T}$ matrix of the complete small-signal model in (5). The eigenvalues provide information about stability and the dynamics modes of the system, with special interest to the oscillatory modes, which are related to complex eigenvalues. In particular, the frequency and the damping ratio of the oscillation modes λ_i are obtained as $f_i = \Im(\lambda_i)/(2\pi)$ and $\xi_i = -\Re(\lambda_i)/|\lambda_i|$. Unstable eigenvalues are related to a negative damping, while positive values close to zero are identified as potential modes to be destabilized in case of different operation conditions or control parameters.

The PFs measure the relative contribution that a state variable has on a mode. Therefore, if the state variables are grouped as explained in Section 2.4.1, interactions can be identified between different parts of the system according to the PFs of the state variables from each group. The PFs has been normalized between 0 (no participation) and 1 (maximum participation) for each mode. Then, it is assumed that a variable has a significant effect on a mode when the associated PF is greater than 0.3 [16].

The dynamic analysis is focused on the impact that the PPC has on the interactions and stability of a LS-PVPP. This analysis represents a first step before an adequate control design of the PPC. Therefore, different scenarios are defined considering variations in the PPC parameters, which includes the active and reactive power controls and the frequency and voltage support. Also, the scenarios should consider the reduction of synchronous generation in the grid, i.e. a power system with high penetration of power electronics. As a result, the following case studies are defined:

- Initial case: The first case study is focused on the PPC analysis considering only active and reactive power controls.
- Analysis of frequency and voltage support: This second case study considers the impact that frequency and voltage droop gains has on the system dynamics.
- Analysis of SG reduction: This last case study considers an eventual reduction of SG that is compensated with an increase of PV generation.

It should be noted that different operating conditions are not considered in this analysis for simplicity. This is because the main purpose of this study is to identify and understand the origin of the main interactions in a LS-PVPP due to the PPC parameters.

The general parameters of the case study are detailed in Appendix A.

3.2. Initial case

This initial case study considers an scenario with a 2 MVA LS-PVPP and a 5 MVA SG that are supplying power to a 5 MW resistive load, such that the LS-PVPP provides 70% and the SG 30% of the total load. A general presentation of all the LS-PVPP modes is provided to identify potential unstable interactions when the PPC is implemented only with active and reactive power controls. Fig. 7 shows the details of each pole, indicating: frequency and damping ratio (only for oscillatory modes), real part and PF contribution (marked with grey groups of variables with PFs higher than 0.3). The state variables are aggregated depending on the group where they belong, according to the definitions in Section 2.4.1, and following the colour representation from Fig. 5.

It is observed that the high frequency modes are related to the grid states, while the low frequency modes are related to the control systems,

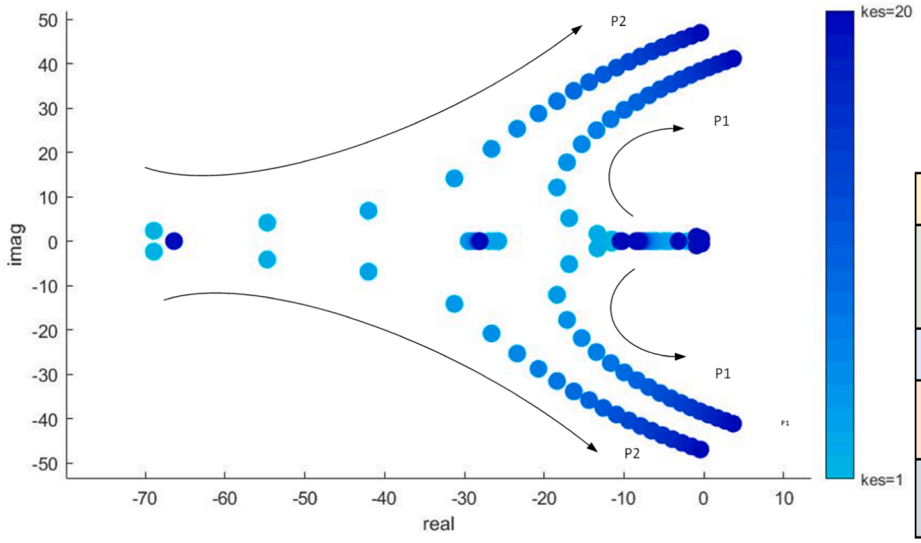

		Kes=1		kes=16		kes=18	
		P1	P2	P1	P2	P1	P2
	f (Hz)	0.059	0.375	6.099	6.959	6.343	7.237
	damp	0.999	0.999	0.013	0.118	-0.04	0.06
	real	-11.5	-68.9	-0.49	-5.2	1.679	-2.72
	----	----	----	----	----	----	----
GRID	Currents						
	Voltages						
VSC	C. loop						
	P loop						
	Q loop						
	PLL						
PPC	Q loop						
	P loop						
Delays	App						
	Meas						
	Com						
SG	Gov						
	Exc						
	SG						

(a) Pole diagram (b) Participation factors

Fig. 8. Relevant modes and associated PFs of the initial case scenario when the PPC control gains are increased.

	Oscillation Modes	1-2	3-4	5-6	7-8	9-10	11-12-13-14	15-16	17-18-19-20	21-22	23-24	25-26	27-28	29-30	31-32	33-34	35-36	37-38
	f (Hz)	1123	1082	1017	979.1	57.72	51.32	50.02	23.81	7.788	1.341	0.16	0.1	0.097	0.09	0.065	0.059	0.031
	damp	0.029	0.118	0.043	0.144	0.963	0.999	0.925	0.507	0.999	0.999	0.653	0.985	0.472	0.999	0.999	0.999	0.999
	real	-207	-810	-273	-896	-1305	-98491	-763	-88	-1038	-1024	-0.87	-3.55	-0.33	-66.2	-157	-12.1	-157
	------	------	------	------	------	------	------	------	------	------	------	F2/V4	V1	F3	------	------	------	------
GRID	Currents	■	■	■	■			■		■	■							
	Voltages	■	■	■	■													
VSC	C. loop															■		■
	P loop																■	
	Q loop																■	
	PLL								■									
PPC	PLL																	
	Q loop																■	
	P loop																■	
Delays	App																	
	Meas						■								■			
	Com														■			
SG	Gov													■				
	Exc											■			■			
	SG					■			■	■		■	■	■	■		■	

	Oscillation Modes	39	40	41	42	24	44	45	46	47	48
	f (Hz)	0	0	0	0	0	0	0	0	0	0
	damp	1	1	1	1	1	1	1	1	1	1
	real	-130	-129	-68.8	-100	-27.1	-10.5	-10.3	-1.9	-1.33	-0.34
	------	------	------	------	------	------	------	------	V2	F1/V3	F4
GRID	Currents										
	Voltages										
VSC	C. loop										
	P loop							■			
	Q loop						■				
	PLL										
PPC	PLL										■
	Q loop									■	
	P loop										
Delays	App										
	Meas	■	■	■	■						
	Com	■	■	■							
SG	Gov										
	Exc										
	SG					■			■	■	■

(a) Oscillatory modes (b) Non-oscillatory modes

Fig. 9. List of LS-PVPP modes and significant PF contribution for the initial case study when frequency and voltage support are analyzed.

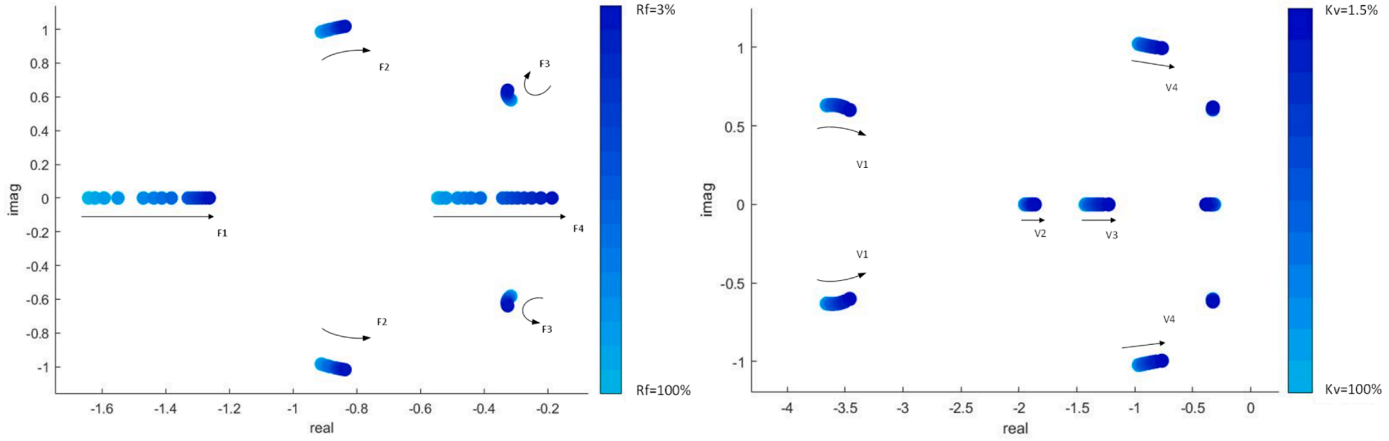

(a) Pole diagram for frequency droop variation (b) Pole diagram for voltage droop variation

Fig. 10. Relevant modes of initial case scenario when frequency and voltage droop percentages are modified.

	Oscillation Modes	1-2	3-4	5-6	7-8	9-10-11-12	13-14	15-16	17-18	19-20	21-22	23-24	25-26	27-28	29-30	31-32	33-34	35-36	37-38
	f (Hz)	1125	1022	974.4	873.6	51.037	50.01	49.01	23.73	23.53	2.81	1.317	0.141	0.114	0.105	0.091	0.063	0.055	0.031
	damp	0.031	0.04	0.222	0.257	1	0.925	0.997	0.518	0.531	1	1	0.804	0.983	1	0.534	0.999	0.999	0.999
	real	-218	-258	-1391	-1462	-98494	-763	-3936	-90.2	-92.6	-1043	-1024	-1.2	-3.78	-65.8	-0.36	-157	-12	-157
	------	------	------	------	------	------	------	S1	------	------	------	------	S2	------	------	S3	------	------	------
GRID	Currents																		
	Voltages																		
VSC	C. loop																		
	P loop																		
	Q loop																		
	PLL																		
PPC	PLL																		
	Q loop																		
	P loop																		
Delays	App																		
	Meas																		
	Com																		
SG	Gov																		
	Exc																		
	SG																		

(a) Oscillatory modes

	Oscillation Modes	39	40	41	42	43	44	45	46	47	48
	f (Hz)	0	0	0	0	0	0	0	0	0	0
	damp	1	1	1	1	1	1	1	1	1	1
	real	-131	-128	-68.4	-100	-26.3	-10.2	-10.3	-1.94	-1.77	-0.14
	------	------	------	------	------	------	------	------	------	------	------
GRID	Currents										
	Voltages										
VSC	C. loop										
	P loop										
	Q loop										
	PLL										
PPC	PLL										
	Q loop										
	P loop										
Delays	App										
	Meas										
	Com										
SG	Gov										
	Exc										
	SG										

(b) Non-oscillatory modes

Fig. 11. List of LS-PVPP modes and significant PF contribution for the modified case study (with a 2 MW load) when frequency and voltage support are analyzed.

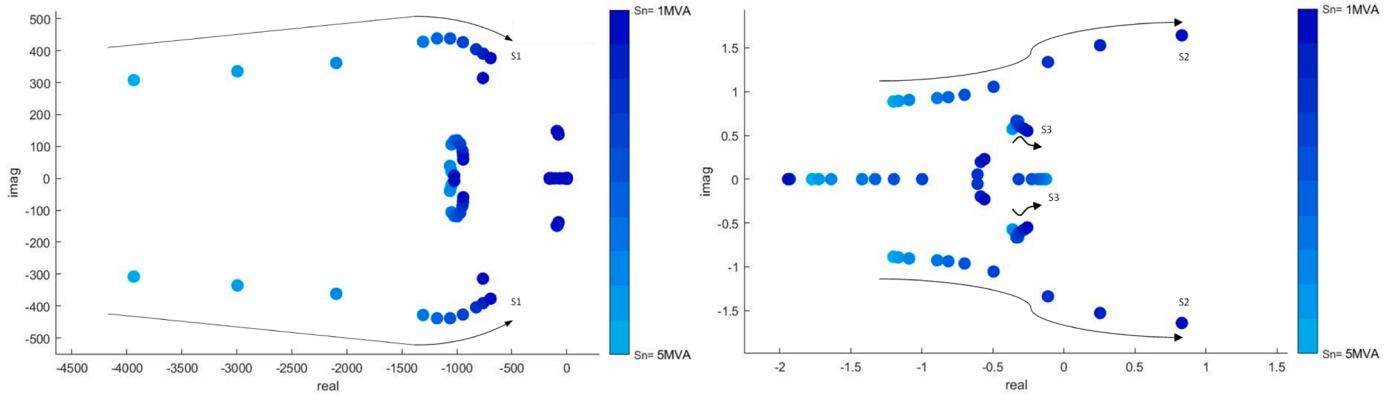

(a) Identification of S1 (b) Identification of S2 and S3

Fig. 12. Relevant modes for modified case scenario when SG nominal power is reduced.

		Sn=5 MVA			Sn=4 MVA			Sn=3 MVA			Sn=2 MVA			Sn=1 MVA		
	Oscillation Modes	S1	S2	S3	S1	S2	S3	S1	S2	S3	S1	S2	S3	S1	S2	S3
	f (Hz)	49.01	0.141	0.091	53.39	0.142	0.091	57.55	0.144	0.092	68.12	0.147	0.1	59.99	0.261	0.088
	damp	0.997	0.804	0.534	0.994	0.793	0.534	0.985	0.769	0.524	0.95	0.693	0.464	0.879	-0.45	0.422
	real	-3936	-1.2	-0.36	-2994	-1.16	-0.36	-2096	-1.09	-0.36	-1307	-0.89	-0.33	-693	0.831	-0.26
	------	-----	-----	-----	-----	-----	------	-----	-----	-----	-----	-----	-----	-----	-----	-----
SG	Gov															
	Exc															
	SG															

Fig. 13. PFs of relevant modes for modified case scenario when SG nominal power is reduced.

delays and SG. Also, interactions can be identified for modes with participation of at least two different groups. In particular, the following interactions are observed:

- SG and VSCs: interaction at 24 Hz (poles 17, 18, 19 and 20)
- SG and the collection grid: interaction at 8 Hz (poles 21 and 22).
- VSC, PPC and SG: interaction at 0.06 Hz (poles 35 and 36).
- SG and PPC: interaction in a non-oscillatory mode (pole 44).

Once the initial poles are identified, an increase of active and reactive power controller gains is applied for representing a future scenario with a faster PPC response. The initial PPC controller gains are designed to achieve the reference value with a settling time of 2 s ($\tau = 0.5$ s). Then, the gains are multiplied by a constant k_{es} until the system is unstable.

Fig. 8 a shows the relevant modes (P1 and P2 indicated in Fig. 7) that are shifted closer to the imaginary axis, i.e. the stability limit. In particular, P1 is the first to cause instability when $k_{es} = 16.6$. Fig. 8b shows the PFs of P1 and P2 for different values of k_{es}. It clear that for low values of k_{es} P1 has relevant participation from the VSC power controls,

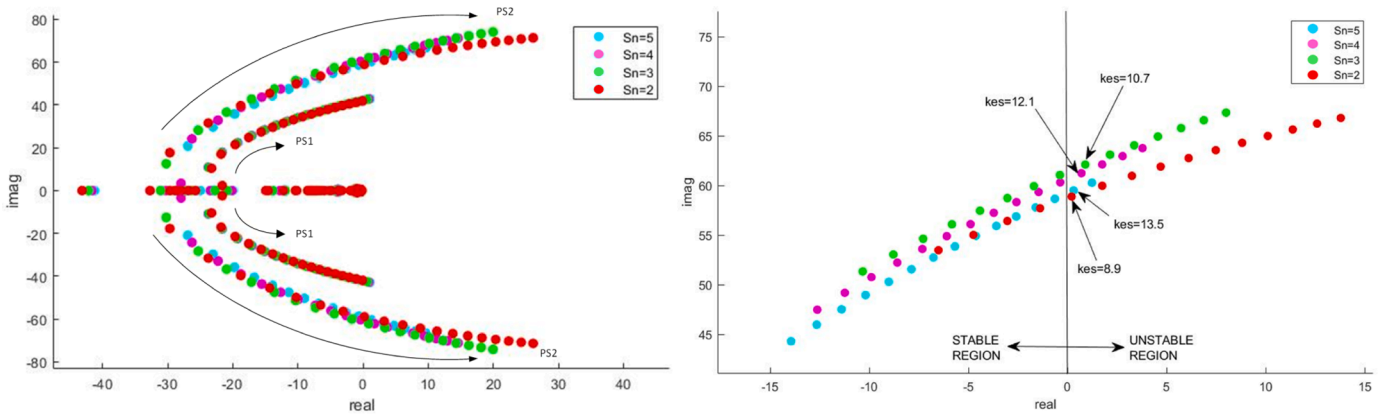

(a) PS1 and PS2 (b) Detail of PS2 around imaginary axis

Fig. 14. Relevant modes for modified case scenario when PPC gains are increased and different values of SG nominal power are considered.

	Sn(SG)	5 MVA		4 MVA		3 MVA		2MVA	
	Oscillation mode	PS1	PS2	PS1	PS2	PS1	PS2	PS1	PS2
	f (Hz)	4.52	75.644	4.50373111	8.08139379	4.4669489	8.69595203	4.36570411	8.98194728
	damp	0.4677	0.2335	0.47194434	0.19145806	0.47898408	0.13236429	0.49556805	0.0538772
	real	-15.04	-11.41	-15.14	-9.9	-15.3145655	-7.29635642	-15.6506752	-3.04499541
	kes	8	8	8	8	8	8	8	8
GRID	Currents								
	Voltages								
VSC	C.loop								
	P loop								
	Q loop								
	PLL								
PPC	PLL								
	Q loop								
	P loop								
Delays	App								
	Meas								
	Com								
SG	Gov								
	Exc								
	SG								

Fig. 15. PFs of relevant modes for modified case scenario when PPC gains are increased and different values of SG nominal power are considered.

the PPC and the SG, while P2 has relevant participation from the measurement and communication delays. Then, when k_{es} increases and is closed to the instability region, P1 also has relevant participation of the measurement and communication delays, while P2 also has participation from the VSC power control and the SG. As a conclusion, when the PPC control gains are increased an instability is originated due to the interaction of the VSC, PPC, system delays and SG.

3.3. Analysis of frequency and voltage support

The introduction of the frequency and voltage support results in the modes shown in Fig. 9. In this case the droop percentages are defined as $R_f = 5\%$ and $R_v = 3\%$. It is observed that two additional modes (poles 42 and 48) are introduced. Pole 42 is mainly related with the measurement delay of the voltage at the PCC, while pole 48 is mainly related to the PLL of the PPC used to calculate the grid frequency. Compared to the modes of the Initial case, an additional interaction between the SG and the system delays is introduced (poles 31 and 32).

Then, the impact that different frequency and voltage droops has on the stability is analysed. The frequency droop percentage is reduced from 100%, which is equivalent to a case without frequency support, to 3%. Fig. 10a shows the most relevant modes (F1–F4 in Fig. 9) according to their mobility towards the unstable region. The voltage droop percentage is also reduced from 100%, which is equivalent to a case without voltage support, to 1.5%. Fig. 10b shows the associated relevant modes (V1–V4 in Fig. 9). It is clear that the mode mobility is limited, which does not affect stability for a large range of frequency or voltage droop percentages. Also, it is observed that F2&V4 and F1&V3 represent the same modes.

In addition, the PFs of these modes can be analysed. In particular, the PFs for high values of R_f and R_v are equivalent to the Initial case (results in Fig. 7), while the PFs for low values of droop percentages are approximately equal to the results in Fig. 9. It is observed that the relevant modes are related to the SG (F2&V4, V1, F3 and V2) and to

Table A1
LS-PVPP model parameters.

Parameter	Value
PV inverters	
Nominal power, S_n	1 MVA
Nominal AC and DC voltages, V_{AC-n} and V_{DC-n}	400 V and 800 V
AC filter (expressed at MV), R_c, L_c and C_f	20 Ω, 0.127 H and 420 μF
PLL time constant, τ_{pll}	0.025 s
Current control time constant, τ_{CL}	0.01 s
Power control time constant, τ_{DC}	0.1 s
Application delay time constant, τ_{app}	10 μs
Collector grid and delays	
Nominal medium voltage, V_n^{MV}	20 kV
Nominal high voltage, V_n^{HV}	200 kV
LV-MV transformer impedance, $\underline{z}_{tr}^{LV-MV}$	$4 \times 10^{-4} + j0.1$ pu
Collector cable impedance, $\underline{z}_{cb}^{coll}$	$0.0034 + j0.0014$ pu/km
Collector cable length, l_{cab}	0.5 km
MV-HV transformer impedance, $\underline{z}_{tr}^{MV-HV}$	$5 \times 10^{-4} + j0.0015$ pu
Communication delay time constant, τ_{com}	20 ms
Measurement delay time constant, τ_{meas}	20 ms
PPC samping delay time constant, τ_{PPC}	20 ms

interactions of the SG with the PPC (F1&V3 and F4).

Therefore, the frequency and voltage support do not have a significant impact in the stability for the load and generation scenario defined in the Initial case. However, some relevant modes represent interactions between SG and PPC, which must be considered for different load and generation scenarios.

3.4. Analysis of SG reduction

The main purpose is to identify the stability limits of a power system with high penetration of PV generation with power electronics. It is expected that renewable generation will replace conventional fossil-fuel options, i.e. a scenario with a decrease of SG nominal power is employed to represent an eventual disconnection of SG units from the grid. Such decreased of SG results in a reduction of inertia and grid strength. Also, the dynamics interactions are analysed for scenarios with reduced SG considering an increase of active and reactive power controller gains, as in the previous subsection. In this direction the SG nominal power is gradually decreased to represent a reduction of synchronous generation in the grid.

Considering the generation and load distribution of the Initial case, a significant reduction of SG nominal power is not possible. Therefore, the power flow is modified such that, the load is reduced from 5 MW to 2 MW and is equally supplied by the LS-PVPP and the SG, i.e. each element provides 50% of the total load. This new power flow distribution allows an SG nominal power reduction down to 1 MVA keeping an equal power supply from the SG and the LS-PVPP, which will be sufficient to analyse the effect that SG nominal power reduction has on the stability.

Fig. 11 shows the modified modes of the system, where the poles and related PFs are slightly different compared to the previous results in Fig. 9. Therefore, it is validated that the new power flow distribution between the LS-PVPP and the SG does not significantly affect the results from the previous sections. In addition, it should be mentioned that variations of load and SG nominal power are not equivalent since the load modification does not affect both the inertia and grid strength.

Once the modified scenario is validated, the SG nominal power is reduced from 5 MVA to 1 MVA (from 5 MVA to 2 MVA with a reduction of 1 MVA, from 2 MVA to 1.2 MVA with a reduction of 0.2 MVA, 1.1 MVA and 1 MVA). Fig. 12 shows the relevant modes (S1–S3 in Fig. 11) and Fig. 13 the related PFs. Instability is detected due to the mode S2 for low SG nominal powers (between 1.2 and 1.1 MVA) and the participation is mainly from SG variables.

The PPC controller gains are also modified as in the Initial case for different SG nominal powers. In particular, the controller gains are multiplied by a constant k_{es} with values from 1 to 20, while the SG nominal power is reduced from 5 to 2 MVA. Fig. 14 shows the mobility of the relevant modes (PS1 and PS2), which are the same modes identified in the Initial case (P1 and P2). In particular, PS2 is causing the system instability for any SG nominal power. In addition, it is observed that for reduced SGs the instability occurs for lower values of k_{es}. Therefore, the PPC time response is more limited for a reduced size of SG.

The PFs of the relevant modes in Fig. 15 when $k_{es} = 8$ show that the participation of PS2 is mainly from the SG variables independently of the SG size, while P2 in the Initial case had participation from VSC, SG and delays. Then, the effect that PPC time response has on the pole mobility is similar to the Initial case, but the PFs are significantly different.

The frequency and voltage support have introduced an additional coupling between the PPC and the SG that lead to different PFs for the relevant mode P2–PS2. However, the PFs of that mode do not show an interaction as significant participation of multiple components. It can be observed that frequency and voltage support are based on proportional controls that do not represent state variables. Therefore, interactions between PPC and SG might not be identified from the PFs, because state variables are not related to the frequency and voltage controls.

4. Conclusions

This paper has presented a small-signal model of a Large Scale Photovoltaic Power Plant connected to the grid in order to analyse potential dynamic interactions that could lead to instability. A sensibility analysis based on eigenvalues and participation factors was used to identify the problematic modes and the contribution of grid components. Two future scenarios where explored: Power Plant Controllers (PPC) with fast dynamic response and a high penetration of power electronics from a reduction of existing Synchronous Generation (SG).

An eventual increase of the PPC response without considering the frequency and voltage support resulted in an instability caused by the interaction of the PV inverters, the PPC and delay effects. This interaction was identified for a low frequency range (below 10 Hz). The introduction of frequency and voltage support introduced an additional coupling between the PPC and the SG. The variation of droop percentages did not impact the stability for the power flow distribution that has been analysed, but interactions between PPC and SG where identified at very low frequencies (below 1 Hz). Also, these additional control loops modified the instability characterization when the PPC response increases, but the interaction was still around the same frequency (below 10 Hz). In particular, the participation factors show a significant contribution of the SG, i.e. interaction between the PPC and the SG is not identified. Also, the reduction of SG resulted in another instability at very low frequency (below 1 Hz) again with significant participation of the SG.

According to the participation factors, these two instabilities are not related to interactions between the SG and PPC. However, it is clear that the introduction of frequency and voltage controls have modified the system dynamics. Therefore, in this case the participation factors might not capture the interactions between the SG and the PPC. Other analysis tools should be used for further insights in these instabilities.

CRediT authorship contribution statement

Ruben Salazar-Chiralt: Conceptualization, Methodology, Software, Visualization, Writing – original draft. **Marc Cheah-Mane:** Writing – original draft, Writing – review & editing, Visualization, Supervision. **Elia Mateu-Barriendos:** Methodology. **Eduard Bullich-Massague:** Conceptualization. **Eduardo Prieto-Araujo:** Conceptualization. **Hasan Mehrjerdi:** Funding acquisition. **Oriol Gomis-Bellmunt:** Writing – original draft, Writing – review & editing, Project administration.

Declaration of Competing Interest

The authors declare that they have no known competing financial interests or personal relationships that could have appeared to influence the work reported in this paper.

Acknowledgements

This work was supported by the National Priorities Research Program under Grant 11S-1125-170027 from the Qatar National Research Fund (a member of Qatar Foundation).

This work is also supported under the umbrella of SOLAR-ERA.NET Cofund, which includes the Ministry of Economy and Competitiveness, the CDTI and the Swedish Energy Agency. SOLAR-ERA.NET is supported by the European Commission within the EU Framework Programme for Research and Innovation HORIZON 2020 (Cofund ERA-NET Action, no. 691664)

The work of Oriol Gomis-Bellmunt is supported by the ICREA Academia program. Marc Cheah-Mane, Eduardo Bullich-Massague and Eduardo Prieto-Araujo are Lecturers of the Serra Hunter programme.

Appendix A. Case study parameters

The LS-PVPP parameters are in Table A.1, while the SG parameters are from Collados-Rodriguez et al. [16].

References

[1] IRENA, Renewable Energy Generation Cost in 2019, International Renewable Energy Agency, 2020.
[2] A. Cabrera-Tobar, E. Bullich-Massagué, M. Aragüés-Peñalba, O. Gomis-Bellmunt, Review of advanced grid requirements for the integration of large scale photovoltaic power plants in the transmission system, Renew. Sustain. Energy Rev. 62 (2016) 971–987.
[3] T.K. Vrana, A. Attya, L. Trilla, Future-oriented generic grid code regarding wind power plants in Europe, Int. J. Electr. Power Energy Syst. 125 (2021) 106490.
[4] B.-I. Crăciun, T. Kerekes, D. Séra, R. Teodorescu, Frequency support functions in large PV power plants with active power reserves, IEEE J. Emerg. Sel. Top. Power Electron. 2 (4) (2014) 849–858.
[5] R.K. Varma, M. Akbari, Simultaneous fast frequency control and power oscillation damping by utilizing PV solar system as PV-STATCOM, IEEE Trans. Sustain. Energy 11 (1) (2020) 415–425.
[6] S.I. Nanou, A.G. Papakonstantinou, S.A. Papathanassiou, A generic model of two-stage grid-connected PVsystems with primary frequency response and inertia emulation, Electr. Power Syst. Res. 127 (2015) 186–196.
[7] A. Ryu, H. Ishii, Y. Hayashi, Battery smoothing control for photovoltaic system using short-term forecast with total sky images, Electr. Power Syst. Res. 190 (2021) 106645.
[8] H.M. Hasanien, An adaptive control strategy for low voltage ride through capability enhancement of grid-connected photovoltaic power plants, IEEE Trans. Power Syst. 31 (4) (2016) 3230–3237.
[9] A. Rosini, D. Mestriner, A. Labella, A. Bonfiglio, R. Procopio, A decentralized approach for frequency and voltage regulation in islanded PV-storage microgrids, Electr. Power Syst. Res. 193 (2021) 106974.
[10] B. Singh, S. Kumar, C. Jain, Damped-SOGI-based control algorithm for solar PVpower generating system, IEEE Trans. Ind. Appl. 53 (3) (2017) 1780–1788.
[11] M. Armendáriz, K. Paridari, E. Wallin, L. Nordström, Comparative study of optimal controller placement considering uncertainty in PV growth and distribution grid expansion, Electr. Power Syst. Res. 155 (2018) 48–57.
[12] H. Liu, L. Jin, D. Le, A.A. Chowdhury, Impact of high penetration of solar photovoltaic generation on power system small signal stability. 2010 International Conference on Power System Technology, 2010, pp. 1–7.
[13] S. Singh, R.K. Verma, A.K. Shakya, S.P. Singh, Frequency stability analysis of hybrid power system based on solar PV with SMEs unit. 2016 International Conference on Emerging Trends in Electrical Electronics Sustainable Energy Systems (ICETEESES), 2016, pp. 5–11.
[14] N.A. Awadhi, M.S.E. Moursi, A novel centralized PV power plant controller for reducing the voltage unbalance factor at transmission level interconnection, IEEE Trans. Energy Convers. 32 (1) (2017) 233–243.
[15] I. Kim, R.G. Harley, Examination of the effect of the reactive power control of photovoltaic systems on electric power grids and the development of a voltage-regulation method that considers feeder impedance sensitivity, Electr. Power Syst. Res. 180 (2020) 106130.
[16] C. Collados-Rodriguez, M. Cheah-Mane, E. Prieto-Araujo, O. Gomis-Bellmunt, Stability analysis of systems with high VSCpenetration: where is the limit? IEEE Trans. Power Deliv. 35 (4) (2020) 2021–2031.
[17] IEEE recommended practice for excitation system models for power system stability studies, IEEE Std 421.5-2016 (Revision of IEEE Std 421.5-2005) (2016) 1–207.